Bull. Egypt. Soc. Physiol. Sci. Vol. (45), Issue (4), 429-448

Bull. of Egyp. Soc. Physiol. Sci.

(Official Journal of Egyptian Society for Physiological Sciences)

(pISSN: 1110-0842; eISSN: 2356-9514)

Protective Potential of Humanin in Renal Ischemia/Reperfusion Injury in Rats: Unveiling Mitochondria-Targeted Mechanisms

Islam Ibrahim Hegab[1,2], Eman H. Basha [1,2], Asmaa H. Okasha[3], Alaa H. Abd El-Azeem[4,] Maram M. Ghabrial [5], Amira M. Abd El Maged[6], Hanan M. Abdallah[1]

1. Physiology Department, Faculty of Medicine, Tanta University, Tanta 31527, Egypt.
2. Bio-Physiology Department, Ibn Sina National College for Medical Studies, Jeddah 22413, Saudi Arabia.
3. Medical Biochemistry Department, Faculty of Medicine, Tanta University, Tanta 31527, Egypt.
4. Medical Pharmacology Department, Faculty of Medicine, Tanta University, Tanta 31527, Egypt.
5. Department of Anatomy & Embryology. Faculty of Medicine, Tanta University, Tanta, Egypt.
6. Department of Pathology, Faculty of Medicine, Menoufia University, Shebin El Kom 32511, Egypt.

Submit Date : 19 Mar. 2025
Accept Date : 25 May 2025

Keywords

- Humanin
- renal ischemia/reperfusion injury
- mitochondrial dysfunction

Abstract

Background: Renal ischemia-reperfusion injury (IRI) is an intricate clinical pathophysiological phenomenon in which oxidative stress, apoptosis, and mitochondrial dysfunction play crucial roles. **Aim**: Validating the effect of humanin (HN) on kidney function in a renal IRI rat model, using its synthetic analogue, S14G-humanin (HNG). **Methodology:** Forty male Wistar rats were categorized into sham, HNG, IR, and IR-HNG groups. Renal function and histopathological analysis were valued to estimate the pathological renal injury. Mitochondrial function was judged by measuring ATP production, mitochondrial transmembrane potential ($\Delta\Psi m$), the electron transport chain (ETC) enzyme complex-I activity, and mitochondrial mitophagy-related genes of Drp1 and Mfn2. Redox, inflammation, and apoptosis biomarkers were scrutinized. The renal PGC-1α, PI3K, AKT, and HIF-1α, coupled with P-JAK2, and P-STAT3 3 were evaluated. Bcl-2 and SIRT1 immunoreactivity were assessed. **Results:** Our findings elucidated that HNG's reno-protective potential against IR-elicited renal damage and mitochondrial dysfunction is mostly mediated via activating the renal SIRT1 / PGC-1α, PI3K/AKT/ HIF-1α, and JAK2/STAT3 signaling. By targeting these crucial pathways, HNG could dampen the renal IR-provoked oxidative stress, inflammation, and apoptosis, and enhance mitochondrial mitophagy and biogenesis. Accordingly, HNG could be a promising therapeutic candidate for renal pathology allied with IRI.

Corresponding author: Islam Ibrahim Hegab, Email:islam.hegab@med.tanta.edu.eg, **TEL:** +966569924666
ORCID:https://orcid.org/0000-0003-1469-1941,

Introduction

Renal ischemia-reperfusion injury (IRI), a major contributor to acute renal failure, is frequently encountered in urological surgeries and kidney transplantations, presenting a significant threat with high morbidity and mortality rates **(1).** Despite impressive medical advancements, the therapeutics available for renal IRI are still scarce **(2).**

Renal IRI has a complex pathophysiology with several participating factors. The generated renal inflammatory cytokines, oxidative stress, injured tubular epithelium, and endothelial dysfunction all contribute to renal structural and functional derangements **(2).**

Renal ischemia triggers mitochondrial dysfunction, ATP depletion, pathological pore formation, and apoptosis **(3).** It disrupts mitochondrial biogenesis by exacerbating mitochondrial fission, causing excessive fragmentation and damage. Fragmented mitochondria generate reactive oxygen species (ROS), serving as the initiator of subsequent renal tissue damage **(4).** In contrast, mitophagy, a subtype of autophagy, targets and eliminates damaged mitochondria, averting excess ROS production, pro-apoptotic factor release, and inflammatory responses **(4).**

The protective role of NAD-dependent deacetylase sirtuin-1 (SIRT1) in renal ischemic injury is well documented, whereas its deficiency aggravates it (5). SIRT1-induced deacetylation of peroxisome/ proliferator-activated/receptor-gamma coactivator (PGC-1α) enhances its nuclear recruitment and transcriptional activation **(5).** PGC-1α, a chief controller of mitochondrial function and biogenesis, governs lipid metabolism and oxidative phosphorylation and modulates ROS generation **(6).**

The phosphatidylinositol-3-kinase (PI3K)/protein kinase/B(AKT)pathway is fundamental in regulating essential cellular functions, involving cell proliferation, survival, apoptosis, and autophagy (7)**.** Activating this pathway safeguards against IRI in various studies **(7, 8).** The oxygen-sensitive transcription factor known as hypoxia-inducible factor-1α (HIF-1α) is crucial for mitochondrial respiration and cellular oxygen balance, and records reno-protective criteria in renal IRI (9)**.**

The Janus kinase (JAK)/signal transducer and activator of transcription (STAT) system offers substantial protection against renal IRI**(2).** Conversely, inhibiting its activation reduces ATP synthesis, escalates ROS levels, and augments cell death in IRI **(10).**

Humanin (HN) is a mitochondrial-derived peptide produced by various body tissues, including the heart, brain, and skeletal muscle. It plays a fundamental role in preventing stress-provoked cell damage, primarily by regulating the intrinsic mitochondrial pathway and exhibiting antioxidant, anti-apoptotic, and anti-inflammatory potential (**11).** S14G-humanin (HNG) is a synthetic HN analogue, engineered by replacing serine at position 14 with glycine, a modification that enhances its biological activity by approximately 1,000-fold compared to native HN **(12).**

Humanin and its analogs proved beneficial in various disease models, including age-related diseases, cardiovascular diseases, and diabetes mellitus **(13).** Nevertheless, limited studies have been conducted to validate HN's protective criterion in renal experimental models. Moreover,

its impact on renal IRI has not been validated yet. Thus, this study is the first to explore the reno-protective potential of HN, using its synthetic HNG analogue in a rat model of renal IRI, paving the way for its potential therapeutic application in various renal pathologies.

2. Materials and methods

2.1 Drugs and Chemicals:

Synthetic humanin analogue (HNG) was obtained from Bucky Labs, Scottsdale, Arizona (CAS # 330936-70-4), and was freshly prepared before administration by dissolving it in normal saline. The study employed high-purity chemicals sourced from Sigma Chemicals Co., St. Louis, MO, USA.

2.2 Surgical model of renal IRI:

Anesthesia for all rats was induced by injecting a ketamine and diazepam combination (75 mg/kg and 5 mg/kg) intraperitoneally (IP)**,** and halothane inhalation (1%) was used to maintain anesthesia **(14).** After executing an abdominal midline laparotomy, the left kidney and its pedicle were isolated from the surrounding adipose tissue, and the left renal artery was clamped with a non-traumatic vascular clamp for 45 minutes, followed by clamp removal to permit reperfusion for 24 hours. Five minutes before the vascular clamp was removed, a right nephrectomy was carried out. A 4-0 silk suture was then utilized to seal the skin layer and abdominal muscles. All surgical procedures were performed under complete aseptic conditions **(14).**

2.3Animal grouping and experimental procedures:

Forty male Wistar rats (220-250 g), acquired from Tanta Medical University's animal house, were kept under 60±5% humidity, 22±2˚C with a 12-hour light/dark cycle, and free water and food access. The execution of animal procedures was carried out with a strict commitment to national guidelines for animal care and was authorized by the local Institutional Animal Ethical Committee, Tanta University's Faculty of Medicine, Egypt (approval No.36264PR488/12/23).

Randomly, rats were allocated to four experimental groups after a week of acclimatization:

i. **Sham group:** Left renal pedicle exploration without ischemia and right nephrectomy. About 0.5 ml of saline vehicle was IP injected.

ii. **HNG-treated group (HNG):** Similar procedure to group I, but they received a single IP HNG injection of (252 µg/kg dissolved in 0.5 ml saline) **(15).**

iii. **IR group:**45 min of left renal ischemia and right nephrectomy **(14)**. About 0.5 ml saline vehicle was IP injected 30 min before the reperfusion period, which was allowed for 24 hours.

iv. **Humanin-treated IR group (HNG-IR):** Similar procedures were conveyed to group III, but they received HNG 252 µg/kg dissolved in 0.5 ml saline via IP injection once, 30 minutes before the reperfusion period, which lasted for 24 hours **(15).**

2.4 Collection of urine, blood, and renal sampling:

After completing the experiment, and for a 24-hour urine collection, each rat was kept in its metabolic cage. Afterward, they were given a large dosage of pentobarbital sodium (40 mg/kg, IP) **(16),** after which they were sacrificed by cervical

dislocation, and blood samples were drawn from the rats' hearts. Centrifugation was used to extract serum from blood samples kept at 20◦C for later biochemical analysis.

Following a midline laparotomy, the left kidney was excised, rinsed with phosphate buffer saline (PBS), and then bisected into 3 portions; for histological and immunohistochemical studies, one portion was fixed in a 10% formaldehyde solution, while, the 2nd portion was wrapped in aluminum foil at – 80o C for molecular assay, and the 3rd portion was divided into 2 sections one for mitochondrial parameters and the other section was centrifuged after being homogenized in PBS (50 mM, pH 7.4), then the supernatant stored at – 80o C for the biochemical studies and their protein concentrations were assessed sticky to the Bradford technique**(17).**

2.5 Biochemical analysis:

2.5.1 Evaluation of Kidney Function.

Serum and urine creatinine were assayed using commercially available kits (Biodiagnostics, Egypt). In addition, the calculation of creatinine clearance (Cr. Cl.) was estimated using the following formula: Cr. Cl. (ml/min) = urine creatinine concentration (mg/dl) x urine volume (ml/24hrs) /plasma creatinine concentration (mg/dl)/1440**(18)**.

Serum levels of neutrophil gelatinase-associated lipocalin (NGAL,Cat#MBS260195, MyBioSource Company, San Diego, USA) and kidney injury molecule-1 (KIM-1), Cat#SEA785Ra, Uscn Life Science Inc., China) were calculated via enzyme-linked immunosorbent assay (ELISA) kits.

2.5.2 Evaluation of redox state (MDA and GSH) and inflammatory cytokines (TNF-a and ICAM-1) in renal tissue.

According to **Ohkawa et al. (19),** malondialdehyde (MDA) levels were assessed in renal tissue by a colorimetric method utilizing thiobarbituric acid (TBA), where the reactive components of TBA were detected at 532 nm. Furthermore, renal reduced glutathione (GSH) concentrations were assayed by the method of **Beutler** (20)**.** The BTS 350 chemical analyzer, a semi-automatic spectrophotometer (Biosystems, Spain), was used to conduct the colorimetric assays. Afterward, levels of intercellular adhesion molecule 1(ICAM-1) and tumor necrosis factor- α (TNF- α) were quantified using MyBioSource rat-specific ELISA kits (Cat# MBS451470 and MBS2507393) respectively.

2.5.3 Assessment of mitochondrial function:

Mitochondrial separation and preservation:

The mitochondria were separated by differential centrifugation, and the total procedure was executed at 4° C to preserve the mitochondria intact. Briefly, the assigned renal portion was homogenized in mitochondrial buffer and centrifuged at 700×g for ten minutes twice. After discarding the supernatant, the mitochondrial pellet was centrifuged for 10 minutes at 7000 x g after being rinsed twice with 5 ml of isolation buffer. A mitochondrial preservation solution containing 1 mM EDTA, 5 mM HEPES, 20 mM sucrose, 100 mM KCl, 10 mM KH2PO4, and 2 mM MgCl2 was used to resuspend the purified mitochondrial pellet, which was then stored on ice for subsequent analysis.

Mitochondrial functional assays:

We used mitochondrial suspension to measure mitochondrial transmembrane potential (ΔΨm) using the methodology of **Maity et al. (21)** to assess changes in ΔΨm using a specific dye as an indicator of mitochondrial health and biogenesis.

Mitochondrial ETC complex enzyme (I) activity and ATP production were also assessed using colorimetric kits provided by Abcam Co. (Cat#ab109721) and Elabscience Co. (Houston, TX, USA) (Cat#E-BC-K157-S), respectively. The specimens' absorbance was measured at 636 nm. The results were adjusted to the protein concentration in the mitochondrial suspension.

2.5.4Assessment of the levels of PI3K and p-JAK2, and p-STAT 3:

The renal homogenate levels of PI3K, p-JAK2, and p-STAT were valued by rat-specific ELISA kits purchased from MyBioSource (Cat#MBS2505796, Cat#MBS7269637, Cat# MBS9900727) respectively. The procedure was executed following the steps outlined in the attached protocol.

2.5.5 Molecular assessment of the mitochondrial mitophagy-related genes: dynamin-related protein 1 (Drp1) and mitofusin2 (Mfn2), caspase 3, PGC1-alpha, Akt, and HIF1α by Real-Time Reverse Transcription PCR (rt–PCR).

Following the manufacturer's steps, the whole RNA was isolated by the Gene JET RNA Purification Kit. A Nanodrop spectrophotometer was employed to judge the RNA quality and quantity. The RNA was reverse transcribed into cDNA using the Revert Aid H Minus Reverse Transcriptase kit. Applying the cDNA as a template, the assigned genes' relative expressions were determined using the Applied Biosystem, Step One Plus RT-PCR system (Thermo Fisher Scientific, SA, Australia). The primers were generated using Primer 5.0 software, with the following rat-specific sequences shown in **(Table 1).** The relative levels of gene expression were determined using the cycle threshold (Ct) technique and standardized to the housekeeping gene **(22).**

Table 1. Sequence-specific primers designed for qRT-PCR

Gene	Forward primer sequence	Reverse sequence	GenBank Accession number
Drp1	5'-GCCCGTGGATGATAAAAGTG-3'	5'-TGGCGGTCAAGATGTCAATA-3'	NM_053655.3
Mfn2	5'-GAGAGGCGATTTGAGGAGTG-3'	5'-CTCTTCCCGCATTTCAAGAC-3'	NM_130894.4
caspase 3	5'-CCCATCACAATCTCACGGTAT-3'	5'-GGACGGAAACAGAACGAACA-3'	NM_012922.2
PGC1-alpha	5'-GGACGAATACCGCAGAGAGT-3'	5'-CCATCATCCCGCAGATTTAC-3'	NM_176075.2
Akt	5'-CGAGTCCCCACTCAACAACT-3'	5'-GGTGAACCTGACCGGAAGTC-3'	NM_033230.2
HIF 1α	5'-CAAAGACAATAGCTTTGCAGAATG-3'	5'-ACGGTCACCTGGTTGCTG-3'	NM_024359.2
GAPDH	5'- AGGTCGGTGTGAACGGATTTG -3'	5'- GGGGTCGTTGATGGCAACA-3'	NM_017008.4

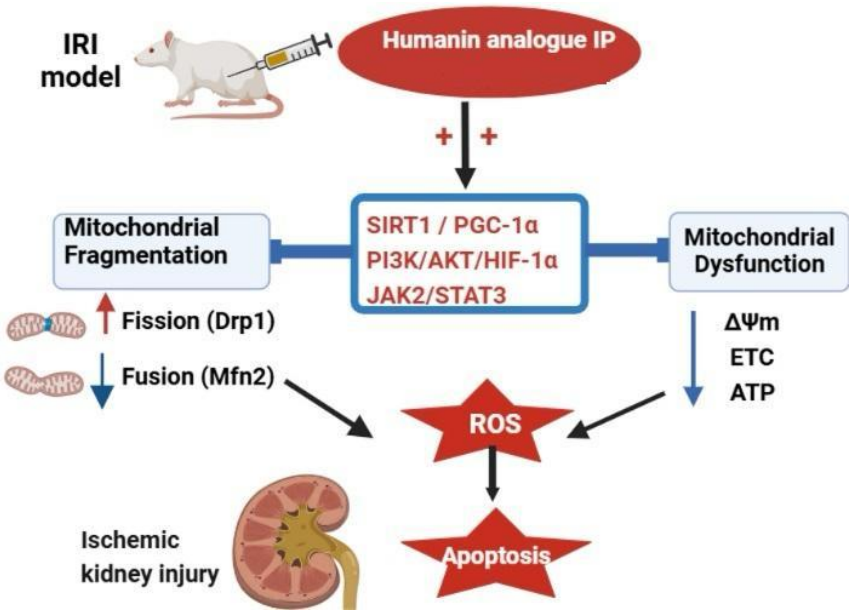

Graphical abstract shows the proposed mechanisms implicated in HNG's potency against renal IRI in rats.

2.5.6 Histological and immunohistochemical studies:

Kidney parts were fixed in 10% formaldehyde solution, dehydrated in ascending alcohol grades, treated with xylol, and submerged in paraffin. A rotatory microtome (Leica, USA) cut five µm-thick sections, which were then exposed to:

2.5.6.1 Hematoxylin and eosin (H&E) stain (23):

Used for studying general histological features.

2.5.6.2 Immunohistochemical staining for detection of B-cell lymphoma-2 (Bcl-2) protein (24):

The avidin-biotin-peroxidase technique was utilized to perform the immunostaining. A rabbit monoclonal Bcl-2 antibody (Sigma Aldrich, Egypt) served as the main antibody.

The secondary antibody was a biotinylated goat antirabbit peroxidase-conjugated antibody (Nova Castra Laboratories Ltd, UK).

Method:

1- The process involved deparaffinizing tissue sections and incubating them in 10% hydrogen peroxide for 15 minutes to dampen peroxidase activity & diminish nonspecific background staining.

2-Sections were soaked in a preheated buffer solution (pH 6), subjected to microwave heat for antigen retrieval for ten minutes, and then allowed to cool for twenty minutes.

3- After two rounds of washing in buffer (0.05% sodium azide), the monoclonal primary antibody Bcl-2α Ab-1 (Ms-123-R7) was applied to the slides.

4- Slides were rinsed four times with 0.05% sodium azide buffer, after which a biotinylated secondary antibody was employed, then incubated at room temperature for ten minutes and washed four times with buffer.

5- After adding the chromogenic substrate, diaminobenzidine (DAB), the mixture was incubated until the desired reaction intensity was

accomplished. Mayer's hematoxylin was used as a counterstain.

6-The Bcl-2 positive cytoplasmic reaction appeared brown, and the nuclei were stained blue.

2.5.6.3 Immunohistochemical staining of paraffin sections for detection of SIRT1(25): kidney specimens were paraffin-embedded and sectioned. A goat serum-blocking solution (Bejing Zhongshan Jinqao Biotechnology Co., Ltd.) was applied dropwise for ten minutes. The samples were incubated overnight at 4°C with Sirt1 primary antibody (1:100). A horseradish peroxidase-conjugated goat anti-mouse IgG 2ryantibody (cat. No. ZDR-5307; 1:300; Bejing Zhongshan Jinqao Biotechnology Co., Ltd.) was incubated with the samples for thirty minutes at room temperature. Each 4-µm section was treated with 50 µl horseradish peroxidase-labeled streptavidin fluid (Beijing Zhongshan Jinqiao Biotechnology Co., Ltd.) followed by three minutes of DAB solution development. The nuclei were counterstained with hematoxylin for forty seconds and then dehydrated. The sections were covered and subjected to microscopic evaluation. The site of the positive reaction was stained brown.

2.5.6.4 Morphometric studies:

The software (Image J) **(National Institutes of Health, Bethesda, Maryland, USA)** was used for measuring the optical density of immunoreactivity in all experimental groups. The optical density of BcL2 and SIRT1 immunoreactivity was measured in Bcl2 and SIRT1 immunohistochemically stained sections, at a magnification of x400.

2.6Statistical analysis:

The mean ± standard deviation was used to depict the collected data. The normality of the data was assessed using the Shapiro-Wilk test. Turkey's post hoc test and one-way ANOVA were conducted to assess the significance. At p-values < 0.05, statistical significance was taken into account. For the statistical studies, GraphPad Prism 8.01 was utilized.

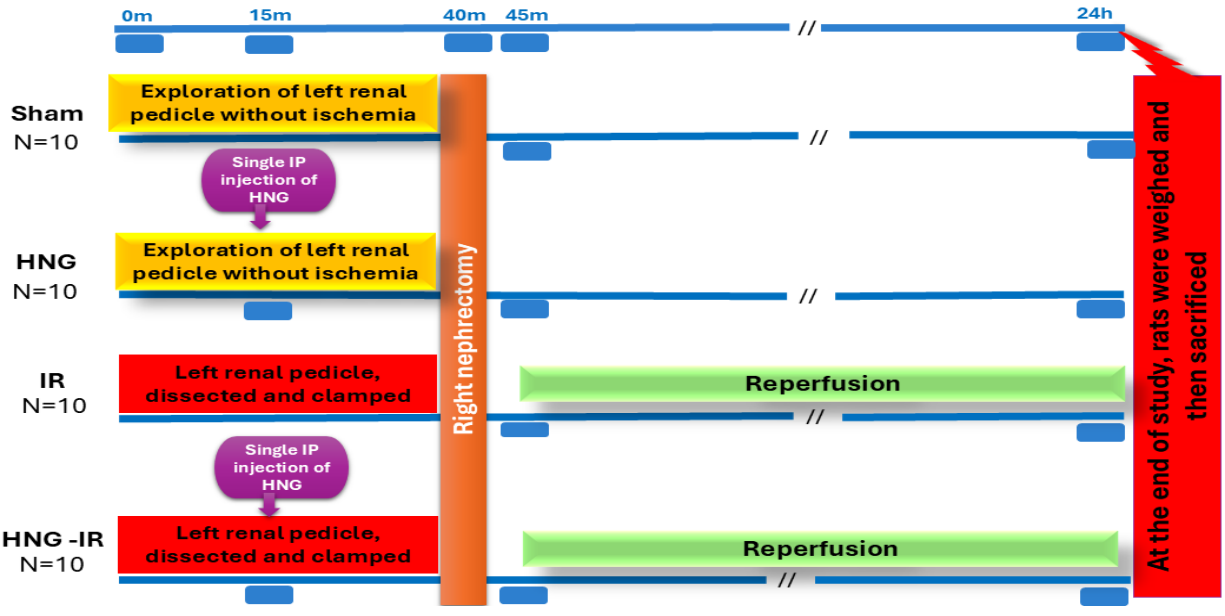

Figure 1. Schematic representation of the whole experimental procedure**.**

3. Results

3.1 Impact of HNG on IR-induced renal dysfunction

As elucidated in **Table 2**, the serum creatinine level was higher, while creatinine clearance was lower, coupled with notably raised serum levels of NAGL and Kim-1 in the IR group against the sham one. Notably, the HNG-IR group revealed a substantial reversal of these abnormalities with an improved renal function comparable to the untreated IR group.

Table 2. Impact of HNG on IR-induced renal dysfunction

	Sham	HNG	IR	HNG-IR
Serum creatinine (mg/dl)	0.47± 0.053	0.45± 0.059	1.69± 0.18$^{*\#}$	0.90±0.105$^{*\#\$}$
Creatinine clearance (ml/min)	2.48±0.37	2.89±0.75	0.47±0.089$^{*\#}$	1.16±0.19$^{*\#\$}$
Serum NAGL (pg/ml)	127.8±9.53	125.0±9.0	285.7±11.52$^{*\#}$	140.0±10.18$^{*\#\$}$
Serum Kim-1 (pg/ml)	75.77±6.51	72.49±6.65	737.6±24.14$^{*\#}$	360±23.9$^{*\#\$}$

p-value-significant (< 0.05), values presented as mean ± SD, (n=10). * Significant from sham group, $^{\#}$ significant from HNG group, $^{\$}$ significant from the IR group. *HNG, humanin analogue; IR, ischemia-reperfusion.; NAGL; Neutrophil gelatinase-associated lipocalin, Kim-1; kidney injury molecule-1.*

3.2 Impact of HNG on IR-induced renal oxidative stress and inflammatory cascade

Figure 2 revealed that renal ischemia prompted a remarkable increment in the renal MDA, TNFα, and ICAM-1 levels and the opposite for the renal GSH levels. In contrast, these parameters were dramatically reversed upon HNG intervention in the HNG-IR group relative to the IR group. This proves its strong antioxidant and anti-inflammatory capabilities in this research.

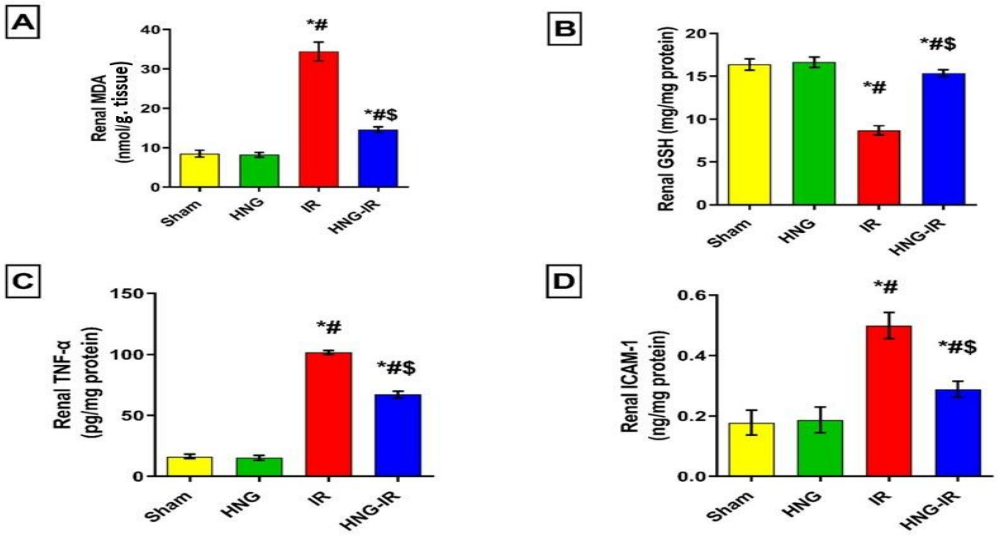

Figure 2. Impact of HNG on the IR provoked oxidative stress and inflammatory cascade

A: Renal MDA (nmol/g tissue). **B.** Renal GSH (mg/mg protein). **C.** Renal TNF-α (pg/mg protein). **D.** Renal ICAM-1 (ng/mg protein). *p*-value-significant (< 0.05), values presented as mean ± SD (n=10). * significant from sham group, $^{\#}$significant from HNG group, $^{\$}$ significant from the IR group. *HNG, humanin analogue; IR, ischemia-reperfusion*; MDA, Malondialdehyde; GSH, Reduced Glutathione; TNF-α, Tumor necrosis factor-alpha; ICAM-1, intercellular adhesion molecule.

3.3 Modulation of HNG to the IR elicited renal mitochondrial dysfunction and associated apoptosis

The results of **Table 3** revealed that the renal mitochondrial parameters (ATP levels, ΔΨm, ETC complex I activity) displayed a noteworthy diminution in the IR group against the sham one. Interestingly, HNG counteracted the renal ischemia's effects on the IR group's measured mitochondrial parameters as revealed by remarkably increased mitochondrial ATP levels, ΔΨm, ETC complex I activity in the HNG-IR group relative to the untreated IR one.

Moreover, the results of **Table 3** revealed that the IR group displayed an imbalance in the mitochondrial mitophagy-related genes with notable Drp1 upregulation and Mfn2 downregulation relative to the sham group. Remarkably, HNG administration restored the mitophagy balance in the HNG-IR group, with a significant reversal of the Drp1, and Mfn2expression to approximate those of the sham group's levels. In the same frame, the IR group notably upregulated the caspase-3 expression differentiated from the sham group. By administering HNG, caspase-3expression levels were dramatically attenuated.

Table 3. Modulation of HNG on the IR elicited renal mitochondrial dysfunction and associated apoptosis

	Sham	HNG	IR	HNG-IR
ATP conc. (nmol/mg protein)	321.7± 22.78	319.5± 20.22	205.5± 18.55$^{*\#}$	270.2±18.26$^{*\#\$}$
ΔΨm (Fluorescence unit)	7.88±0.58	8.06±0.43	2.12±0.27$^{*\#}$	6.76±1.24$^{*\#\$}$
ETC complex enzyme (I) activity (nmol/min/mg protein)	34.52±3.26	32.86±2.49	16.03±1.13$^{*\#}$	22.51±2.29$^{*\#\$}$
Drp1 relative mRNA expression (Fold change)	1.044±0.027	1.043±0.024	1.588±0.051$^{*\#}$	1.148±0.034$^{*\#\$}$
Mfn2 relative mRNA expression (Fold change)	1.045±0.026	1.050±0.027	0.571±0.048$^{*\#}$	0.896±0.050$^{*\#\$}$
Caspase-3 relative mRNA expression (Fold change)	1.021±0.039	1.046±0.035	3.253±0.100$^{*\#}$	2.095±0.060$^{*\#\$}$

p-value-significant (< 0.05), values presented as mean ± SD, (n=10). * significant from sham group, $^{\#}$significant from HNG group, $^{\$}$ significant from the IR group. *HNG, humanin analogue; IR, ischemia-reperfusion.; ATP, Adenosine triphosphate, ΔΨm; mitochondrial transmembrane Potential, ETC; Electron transport chain; Drp1, Dynamin-related protein 1; Mfn2, mitofusin 2.*

3.4 Impact of HNG on the IR-induced alteration in the renal PGC-1α, PI3K/AKT /HIF-1α pathway, and JAK2/STAT 3 system

As depicted in **Figure 3A**, the IR group remarkably downregulated the PGC-1α expression compared with the sham group. By administering HNG, PGC-1αexpression levels were dramatically increased.

Considering that the PI3K/AKT/ HIF-1α pathway contributes an integral reno-protective function in

IRI, we scrutinized their renal levels in all studied groups. **Figure 3(B-D)** depicted that the levels of PI3K and AKT were noticeably lower, while those of HIF-1α were higher versus the sham one. Intriguingly, the HNG-IR group exhibited an enormous rise in all these levels, comparable to the IR group.

Regarding the JAK2/STAT3 pathway, the IR group revealed a distinct increase in their phosphorylated levels relative to the sham one. Interestingly, HNG administration to the HNG-IR group further enhanced their levels in a significant manner comparable to the IR group, as displayed in **Figure 3(E,F).**

3.5 Impact of HNG on the renal histological structure

As displayed in **Figure 4A-B,** the renal cortical sections of the sham & HNG groups exhibited normal histological architecture as glomerulus surrounded by a simple squamous parietal cell layer of Bowman's capsule with Bowman's space. Simple cuboidal epithelium lines the proximal convoluted tubules (PCTs) with a brush border, whereas the distal convoluted tubules (DCTs) are lined by simple cuboidal epithelium.

The renal IR cortical sections presented a disturbance of the normal histological architecture due to renal injury. Shrunken necrotic glomeruli that had lost their cells, and others showing vacuolation with a widening of Bowman's space, were seen. Tubular necrosis in the form of brush border loss with shedding of tubular cells and debris in the lumen, tubular vacuolations, and pyknotic nuclei. Wide intertubular spaces and areas of hemorrhage were also seen as illuminated in **Figure 4C.**

In contrast, the HNG-IR renal cortical sections restored the normal renal histological structure indicated by a normal glomerulus surrounded by Bowman's space with proximal and distal convoluted tubules. However, areas of hemorrhage and some tubules showing vacuolation still appeared, as displayed in **Figure 4D.**

3.6 Impact of HNG on the renal Bcl-2 and SIRT1immunohistochemistry

Figure 5(A-D) presents an assessment of the optical density of bcl2 immunostained sections, revealing that the sham & HNG groups showed positive expression of anti-apoptotic bcl2 in the form of intense brown coloration. Contradictory, the IR group displayed negative reactions of bcl2 relative to both sham and HNG groups. Interestingly, the HNG-IR group showed a substantial increase in bcl2 expression with mild brown staining compared to the IR group.

Moreover, examination of the optical density of SIRT1 immunostained sections revealed that both the sham & HNG groups showed strong brown staining and positive expression. In contrast, the IR group showed negative reactions to SIRT1 relative to the sham and HNG groups. Remarkably, the HNG-IR group showed moderate brown staining and a noteworthy rise in the SIRT1 expression relative to the IR group, as explicated in **Figure 5(E-H)**.

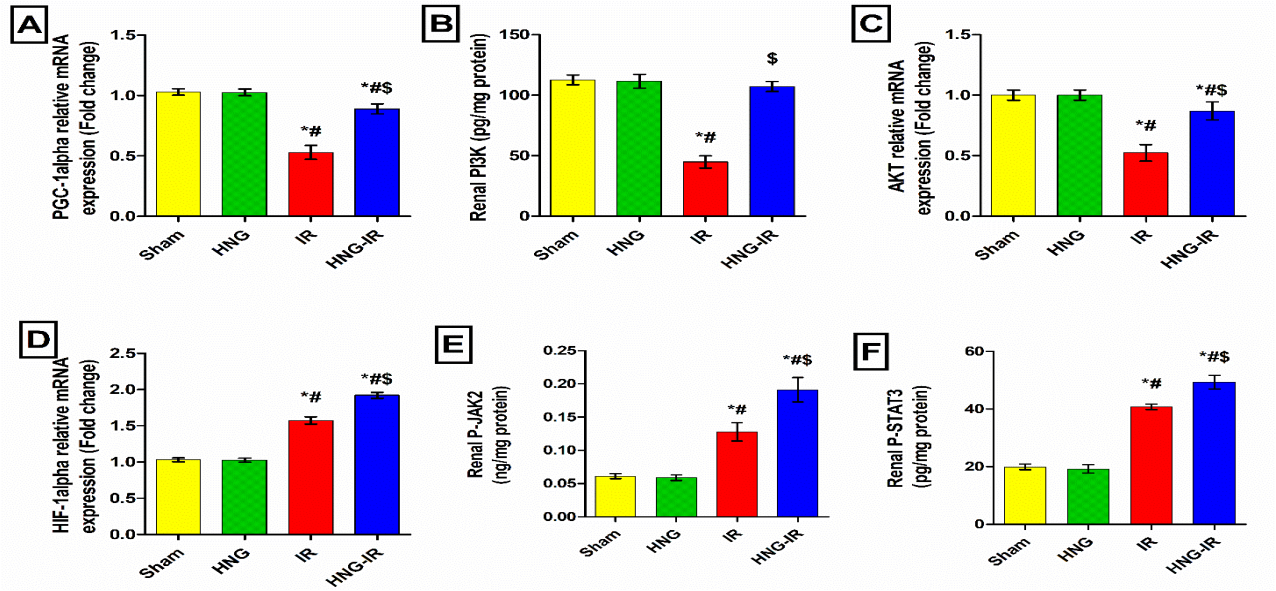

Figure 3. Impact of HNG on the IR-induced alteration in the renalPGC-1α, PI3K/AKT/HIF-1α pathway, and JAK2/STAT 3 system

A: Renal PGC-1α relative mRNA expression (Fold change), **B:** Renal PI3K (pg/mg protein), **C:** AKT relative mRNA expression, **D:** HIF-1α relative mRNA expression, **E**: Renal P-JAK2 (ng/mg protein), **F:** Renal P-STAT3 (pg/mg protein). *p-value-significant (< 0.05), values presented as mean ± SD (n=10).* [*] *significant from sham group,* [#] *significant from HNG group,* [$] *significant from the IR group. HNG, humanin analogue; IR, ischemia-reperfusion; PGC-1α, peroxisome proliferator-activated receptor-γ coactivator 1 alpha; PI3K, phosphatidylinositol 3-kinase; AKT, protein kinase B; HIF1α, Hypoxia-inducible factor 1-alpha; JAK2, Janus kinase 2 gene; STAT3, signal transducer and activator of transcription 3.*

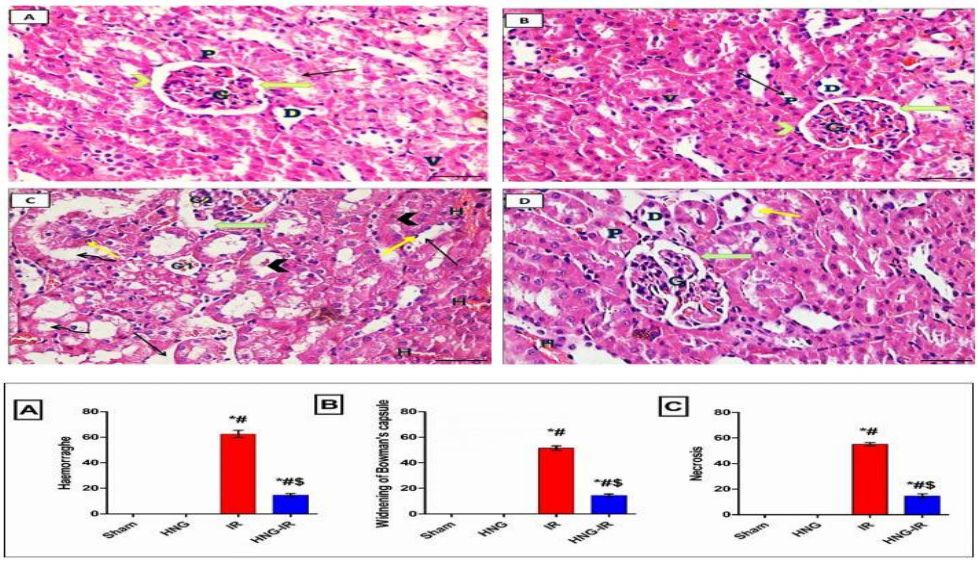

Figure 4. Impact of HNG on the renal histological structure

The renal cortical sections of sham & HNG groups show a normal renal cortical histological architecture as glomerulus (G), surrounded by a simple squamous parietal cell layer (arrow head) of Bowman's capsule and Bowman's space (green arrow) appears. The PCTs (P) are lined by simple cuboidal epithelium with a brush border (black arrow) and DCTs (D) is lined by simple cuboidal epithelium. Interstitial blood vessels (V) appear among the renal tubules **(Fig. 4 A- B).** Section of IR renal cortex revealing disturbance of the normal architecture of the renal cortex due to renal injury. Necrosis of glomeruli that have lost their cells and appear shrunken (G1), another one showing vacuolation (G2) with a widening of Bowman's space (green arrow) are seen. Tubules showed loss of brush border with shedding of tubular cells and casts in the lumen. Tubules also show vacuolations (curved arrow) and pyknotic nuclei (yellow arrows). Wide intertubular spaces (black arrow) and areas of hemorrhage (H) were also seen **(Fig. 4 C).** Section of the renal cortex of the HNG-IR group demonstrated regaining of the normal renal histological structure in the form of the normal glomerulus (G)surrounded by Bowman's space (green arrow), PCTs (P) and DCTs (D). However, areas of hemorrhage (H) and some tubules showing vacuolation (yellow arrow) still appeared **(Fig. 4D)**. Histological scores (Widening of Bowman's capsule, Tubular necrosis & Hemorrhage) **(A- D ×400).** [*] Significant from Sham group, [#] significant from HNG group, [$] significant from IR group.

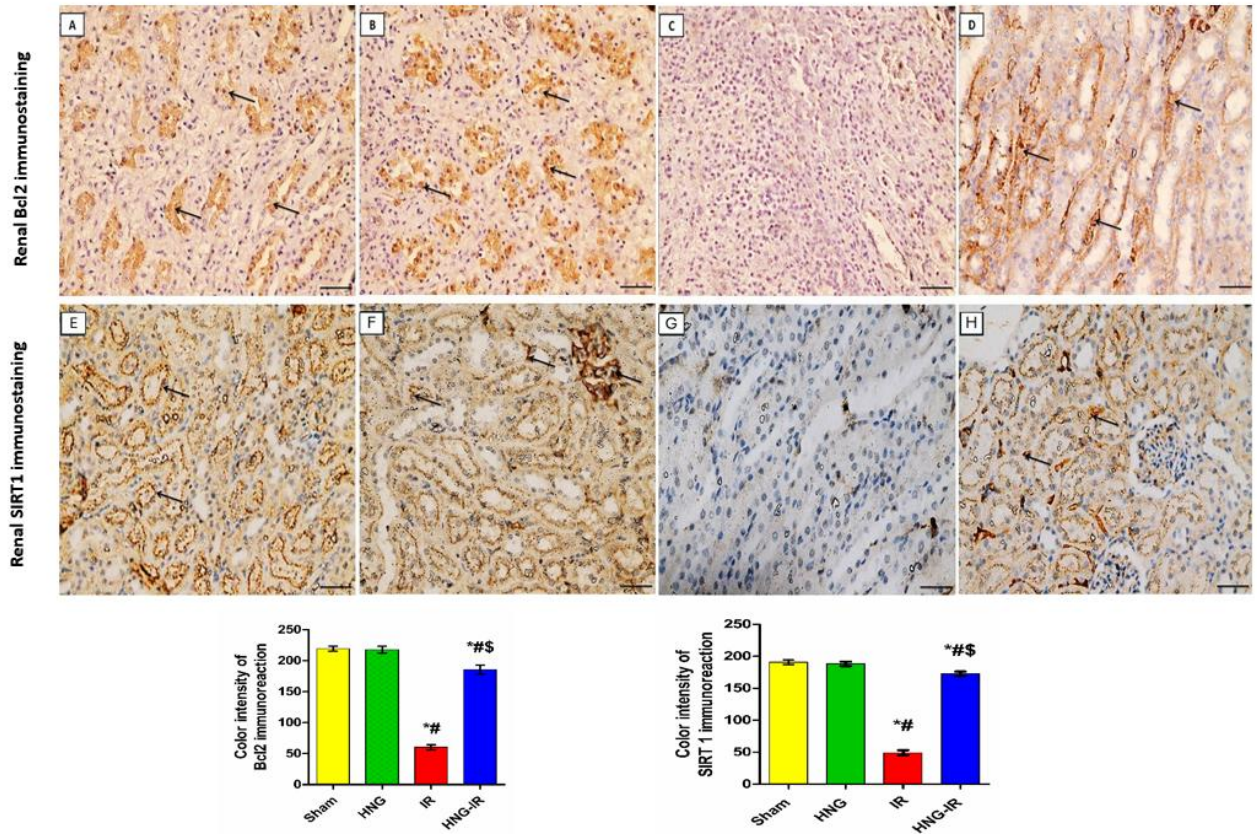

Figure 5. Impact of HNG on renal Bcl2 and SIRT1 immunostaining.
Regarding the Bcl2 immunostaining, **(A & B):** Positive expression of Bcl2 in the sham and HNG groups respectively. **(C):** Negative expression of Bcl2 in the IR group **(D):** Positive Bcl2 expression in the HNG-IR group.
Regarding the SIRT1 immunostaining, **(E & F)**: Positive expression of SIRT1 in the sham and HNG groups respectively. **(G):** Negative expression of SIRT1 in the IR group. **(H):** Positive SIRT1 expression in the HNG-IR group. (black arrows: positive reaction) **(A-H × 400).** The color intensity of BCL2 and SIRT1immunoreaction in immunostained sections for all groups is shown. *Significant from the Sham group, #significant from the HNG group, and $ significant from the IR group.

4. Discussion

Our investigations have validated HNG's alleviation of IR-incited renal dysfunction and injury allied with mitochondrial dysfunction, inflammation, oxidative stress, and apoptosis. HNG's beneficial effects could be possibly mediated via upregulating the SIRT1 / PGC-1α, PI3K/AKT/HIF-1α, besides JAK2/STAT3signaling pathways, illuminating avenues for the mitigating role of HNG in IR-related renal damage. This study, to the best of our knowledge, represents the first documented evidence of HNG's reno-protective potential in the IRI rat model.

In concord with the established IRI pathophysiology **(26, 27),** the IR group exhibited a noteworthy deteriorated renal function, evinced by a remarkable rise in BUN and serum levels of creatinine, NAGL, and KIM-1 along with a reduction in Cr Cl, which was reinforced by the histological picture. In contrast, the HNG-treated group demonstrated a noteworthy improvement in these markers, referring to HNG's anticipated reno-protective impact, as supported previously **(28).**

Interestingly, our investigations clarified that the renal IR-exposed rats displayed raised levels of TNF-α, ICAM-1, and MDA with diminished GSH levels, convincing the IR provoked oxidative stress

and inflammatory response with concurrent renal damage **(29).**

Mitochondrial oxidative stress and dysfunction are crucial pathogenic renal IRI factors. Renal IRI-induced ROS directly damages the mitochondrial respiratory chain, ultimately increasing electron leakage in a vicious circle of ROS formation **(30).** Excess ROS release disrupts the calcium levels and ATP generation and persuades the mitochondrial permeability transition pores [MPTP] to open with a sequel loss of mitochondrial ΔΨm, which provokes apoptosis and necrosis **(31).**

In line with this, a substantial decline in mitochondrial ATP levels, ΔΨm, ETC complex I activity was noted in renal tissue of IR-exposed rats, indicative of mitochondrial dysfunction with loss of membrane potential. Moreover, the mitochondrial fission/fusion balance was disrupted as evidenced by the raised levels of fission protein, Drp1, and declined those of fusion protein, Mfn2, coupled with increased caspase-3levels and decreased Bcl2 immunoreactivity. These data reflected mitochondrial dysfunction and fragmentation with subsequent apoptosis, which verified the IR-induced disruption in mitochondrial redox equilibrium, dynamics, and mitophagy, as consistent with prior research **(6).**

Interestingly, our investigations revealed a significant reversal of all the previously mentioned parameters following HNG treatment. These findings documented HNG's potent antioxidant and anti-inflammatory criteria **(32),** and its efficacy in restoring the mitophagy balance and mitigating mitochondrial dysfunction and fragmentation, which impacted apoptosis and prevented further renal damage. These observations align with existing research in other experimental models **(15, 33, 34).**

To dissect HNG's molecular mechanisms, we assessed the SIRT1/PGC-1α, PI3K/AKT/HIF-1α, and JAK2/STAT 3 signaling pathways to validate their possible involvement in mediating HNG's reno-protective criterion.

Intriguingly, our findings documented that HNG significantly enhanced the SIRT1 immunoreactivity and PGC-1α expressional levels in treated IR rats compared to the untreated counterparts, which was consistent with earlier research **(35–37),**

The SIRT1/PGC-1α pathway activation is well-documented for alleviating mitochondrial dysfunction in renal **(5),** cerebral **(38),** and myocardial **(39)** ischemic injuries. During IRI, PGC-1α safeguards mitochondrial homeostasis by dampening ROS and activating mitochondrial biogenesis **(40).** It governs the quality control mechanisms in the mitochondria, involving fusion, fission, and mitophagy **(41).** By regulating nuclear factor-erythroid 2 related factor 2 (NRF-2), PGC-1α can upregulate antioxidant genes and indirectly influence mitophagy-associated proteins such as Parkin and PTEN-induced putative kinase 1 (40)**.** Thus, HGN's instigation of the SIRT1 / PGC-1α pathway may partly mediate its reno-protective potential in our model.

Following **Kim et al.(42) and Gao et al. (43),** HNG intervention herein displayed a substantial boost of the PI3K/AKT/HIF-1α. This pathway was validated to confer reno-protection against IRI **(44).** Furthermore, exogenous HNG is believed to mitigate mitochondrial biogenesis by enhancing the PI3K/AKT pathway **(45).**

In renal IRI, augmenting the PI3K/Akt/ HIF-1α could boost autophagy and hamper apoptosis, oxidative stress, and the inflammatory cascade **(7, 46, 47).** The enhanced expression of HIF-1α following IR constitutes an endogenous adaptive mechanism that shields the renal cells against ischemic injury **(27).** HIF-1α overexpression can inhibit the IRI-induced ROS generation and apoptosis in tubular cells through mitophagy-mediated mechanisms **(9)**. It can promote autophagy and regulate the tricarboxylic acid cycle in the mitochondria. Moreover, HIF-1α modulates mitochondrial dynamics and inhibits hypoxia-induced mitochondrial fission through heme oxygenase-1 upregulation, potentially preventing tubular injury **(48).**

Noteworthy, our investigations revealed that the IR-challenged kidneys displayed a considerable boost in p-JAK2 and p-STAT3 expression levels, which were further enhanced upon HNG treatment, as formerly observed **(42, 43, 49).**

Activating JAK2/STAT3 has demonstrated promise in mitigating renal IR-associated injury by upregulating protective and anti-apoptotic proteins **(2).** Furthermore, STAT3 regulates mitochondrial bioenergy by influencing the ETC complexes I, II, and V, and inhibiting the MPTP formation by interacting with cyclophilin D, which ultimately stabilizes the mitochondrial ΔΨm and dampens the release of cytokines that provoke apoptosis **(10).** Thus, we could speculate that the HNG's modulatory effect on IR-allied mitochondrial dysfunction and apoptosis may be mediated by activating the JAK2/STAT3 system.

Moreover, the HNG's direct antioxidant criterion proved herein could improve mitochondrial dysfunction and enhance renal cell survival. In this context, **Cai et al. (49)** illuminated that HN exerts its protective effects both intracellularly and extracellularly. **Intracellularly,** HN safeguards mitochondrial function by hindering ETC complexes I and III, impeding ROS formation and fostering the NRF-2 pathway. **Extracellularly**, HN initiates various signaling pathways involving PI3K/AKT and JAK2/STAT3, which promote autophagy and diminish ROS production, contributing to cellular and mitochondrial protection, which matches our findings.

Simultaneously, the direct anti-apoptotic effect of HNG reported previously **(32, 51)** and evinced herein by its instigation of Bcl-2 could dampen ROS release, maintain mitochondrial membrane permeability, and avert caspase-3 activation **(1).** In support, **Means and Katz (50)** elucidated that the Bcl-2 family regulates mitochondrial fission and fusion via interactions with Mfn2 and Drp-1. Drp1 accumulation precedes cytochrome c release, caspase activation, and apoptosis, increasing mitochondrial fission. Meanwhile, Mfn2 overexpression hinders apoptosis, cytochrome c release, and Bax activation. In addition, HN directly binds to Bax, blocking its mitochondrial translocation, hindering cytochrome-c release, ultimately impeding caspase-3 instigation and subsequent cell death **(52).**

Collectively, we propose that the HNG's attenuating impact against IR-induced oxidative stress, inflammation, mitochondrial dysfunction, and associated apoptosis may be mediated through the triggering of the SIRT1/PGC-1α, PI3K/Akt/HIF-1α, and JAK2/STAT3 pathways, which could be enforced by HNG's direct antioxidant and antiapoptotic properties.

5.Conclusions

Our study revealed, **for the first time**, the reno-protective potential of HNG against renal IRI. By triggering the SIRT1 / PGC-1α, PI3K/AKT/HIF-1α, and JAK2/STAT3 signaling pathways, HNG exhibited a remarkable capability to hamper oxidative stress and inflammation, alleviate mitochondrial dysfunction and apoptosis, and restore the disturbed mitochondrial fission/fusion equilibrium, key contributors to renal IRI pathology. This newfound understanding of HNG's molecular mechanisms establishes a foundation for considering it a promising agent in antagonizing renal IRI-associated injury. Further investigation and clinical trials are essential to comprehensively elucidate HNG's therapeutic potential, particularly in perioperative renal protection.

6. Declarations and Statements:

Ethics and statements:

We executed the study protocol following the Local Committee of Research and Medical Ethics of Tanta's Faculty of Medicine.

Availability of data and materials:

The data supporting the outcomes of this study are available from the corresponding author upon reasonable request.

Competing interests: No conflicts of interest were declared by the authors.

Funding: The authors revealed no specific funding for this study

Authors' contributions:

All authors contributed to the data analysis and interpretation, writing–reviewing, and editing of the manuscript, and consented to the final manuscript.

References

1. **Amini N**, **Sarkaki A**, **Dianat M**, **Mard SA**, **Ahangarpour A**, **Badavi M**. The renoprotective effects of naringin and trimetazidine on renal ischemia/reperfusion injury in rats through inhibition of apoptosis and downregulation of micoRNA-10a. Biomedicine & Pharmacotherapy 112: 108568, 2019. doi: 10.1016/j.biopha.2019.01.029.
2. **Liu Y**, **Wang L**, **Du Y**, **Chen Z**, **Guo J**, **Weng X**, **Wang X**, **Wang M**, **Chen D**, **Liu X**. Effects of apigenin pretreatment against renal ischemia/reperfusion injury via activation of the JAK2/STAT3 pathway. Biomedicine & Pharmacotherapy 95: 1799–1808, 2017. doi: 10.1016/j.biopha.2017.09.091.
3. **Bonora M**, **Patergnani S**, **Ramaccini D**, **Morciano G**, **Pedriali G**, **Kahsay A**, **Bouhamida E**, **Giorgi C**, **Wieckowski M**, **Pinton P**. Physiopathology of the Permeability Transition Pore: Molecular Mechanisms in Human Pathology. Biomolecules 10: 998, 2020. doi: 10.3390/biom10070998.
4. **Huang R**, **Zhang C**, **Xiang Z**, **Lin T**, **Ling J**, **Hu H**. Role of mitochondria in renal ischemia–reperfusion injury. FEBS J 291: 5365–5378, 2024. doi: 10.1111/febs.17130.
5. **Funk JA**, **Schnellmann RG**. Accelerated recovery of renal mitochondrial and tubule homeostasis with SIRT1/PGC-1α activation following ischemia–reperfusion injury. Toxicol Appl

Pharmacol 273: 345–354, 2013. doi: 10.1016/j.taap.2013.09.026.

6. **Kobroob A**, **Kongkaew A**, **Wongmekiat O**. Melatonin Reduces Aggravation of Renal Ischemia–Reperfusion Injury in Obese Rats by Maintaining Mitochondrial Homeostasis and Integrity through AMPK/PGC-1α/SIRT3/SOD2 Activation. Curr Issues Mol Biol 45: 8239–8254, 2023. doi: 10.3390/cimb45100520.
7. **Wei Q**, **Zhao J**, **Zhou X**, **Yu L**, **Liu Z**, **Chang Y**. Propofol can suppress renal ischemia-reperfusion injury through the activation of PI3K/AKT/mTOR signal pathway. Gene 708: 14–20, 2019. doi: 10.1016/j.gene.2019.05.023.
8. **Hu S**, **Zhang Y**, **Zhang M**, **Guo Y**, **Yang P**, **Zhang S**, **Simsekyilmaz S**, **Xu J-F**, **Li J**, **Xiang X**, **Yu Q**, **Wang C-Y**. Aloperine Protects Mice against Ischemia-Reperfusion (IR)-Induced Renal Injury by Regulating PI3K/AKT/mTOR Signaling and AP-1 Activity. Molecular Medicine 21: 912–923, 2015. doi: 10.2119/molmed.2015.00056.
9. **Fu Z-J**, **Wang Z-Y**, **Xu L**, **Chen X-H**, **Li X-X**, **Liao W-T**, **Ma H-K**, **Jiang M-D**, **Xu T-T**, **Xu J**, **Shen Y**, **Song B**, **Gao P-J**, **Han W-Q**, **Zhang W**. HIF-1α-BNIP3-mediated mitophagy in tubular cells protects against renal ischemia/reperfusion injury. Redox Biol 36: 101671, 2020. doi: 10.1016/j.redox.2020.101671.
10. **Meier JA**, **Hyun M**, **Cantwell M**, **Raza A**, **Mertens C**, **Raje V**, **Sisler J**, **Tracy E**, **Torres-Odio S**, **Gispert S**, **Shaw PE**, **Baumann H**, **Bandyopadhyay D**, **Takabe K**, **Larner AC**. Stress-induced dynamic regulation of mitochondrial STAT3 and its association with cyclophilin D reduce mitochondrial ROS production. Sci Signal 10, 2017. doi: 10.1126/scisignal.aag2588.
11. **Paharkova V**, **Alvarez G**, **Nakamura H**, **Cohen P**, **Lee K-W**. Rat Humanin is encoded and translated in mitochondria and is localized to the mitochondrial compartment where it regulates ROS production. Mol Cell Endocrinol 413: 96–100, 2015. doi: 10.1016/j.mce.2015.06.015.
12. **Zhang J**, **Lei H**, **Li X**. The protective effects of S14G-humanin (HNG) against mono-sodium urate (MSU) crystals- induced gouty arthritis. Bioengineered 13: 345–356, 2022. doi: 10.1080/21655979.2021.2001911.
13. **Karachaliou C-E**, **Livaniou E**. Neuroprotective Action of Humanin and Humanin Analogues: Research Findings and Perspectives. Biology (Basel) 12: 1534, 2023. doi: 10.3390/biology12121534.
14. **Makled MN**, **El-Awady MS**, **Abdel-Aziz RR**, **Shehab El-Din AB**, **Ammar EM**, **Gameil NM**. Pomegranate extract ameliorates renal ischemia/reperfusion injury in rats via suppressing NF-κB pathway. Hum Exp Toxicol 40: S573–

S582, 2021. doi: 10.1177/09603271211041998.

15. **Abozaid ER**, **Abdel-Kareem RH**, **Habib MA**. A novel beneficial role of humanin on intestinal apoptosis and dysmotility in a rat model of ischemia reperfusion injury. Pflugers Arch 475: 655–666, 2023. doi: 10.1007/s00424-023-02804-0.
16. **Khaled S**, **Makled MN**, **Nader MA**. Tiron protects against nicotine-induced lung and liver injury through antioxidant and anti-inflammatory actions in rats in vivo. Life Sci 260: 118426, 2020. doi: 10.1016/j.lfs.2020.118426.
17. **Bradford M**. A Rapid and Sensitive Method for the Quantitation of Microgram Quantities of Protein Utilizing the Principle of Protein-Dye Binding. Anal Biochem 72: 248–254, 1976. doi: 10.1006/abio.1976.9999.
18. **Akinnuga AM**, **Bamidele O**, **Adewumi AJ**. Evaluation of Kidney Function Parameters in Diabetic Rats Following Virgin Coconut Oil Diet. Folia Med (Plovdiv) 61: 249–257, 2019. doi: 10.2478/folmed-2018-0083.
19. **Ohkawa H**, **Ohishi N**, **Yagi K**. Assay for lipid peroxides in animal tissues by thiobarbituric acid reaction. Anal Biochem 95: 351–358, 1979. doi: 10.1016/0003-2697(79)90738-3.
20. **Beutler E**. Active transport of glutathione disulfide from erythrocytes. Functions of glutathione, biochemical, physiological, toxicological, and clinical aspects. New York, NY, USA: Raven Press, 1983.
21. **Maity P**, **Bindu S**, **Dey S**, **Goyal M**, **Alam A**, **Pal C**, **Mitra K**, **Bandyopadhyay U**. Indomethacin, a Non-steroidal Anti-inflammatory Drug, Develops Gastropathy by Inducing Reactive Oxygen Species-mediated Mitochondrial Pathology and Associated Apoptosis in Gastric Mucosa. Journal of Biological Chemistry 284: 3058–3068, 2009. doi: 10.1074/jbc.M805329200.
22. **Livak KJ**, **Schmittgen TD**. Analysis of Relative Gene Expression Data Using Real-Time Quantitative PCR and the 2−ΔΔCT Method. Methods 25: 402–408, 2001. doi: 10.1006/meth.2001.1262.
23. **Suvarna S K LC and BJD**. Bancroft's Theory and Practice of Histological Techniques. Churchill Livingstone, Elsevier, Philadelphia, 2013, p. 151.
24. **Rajneesh Sharma**. Localization of interleukin-2 in goat ovary. IOSR J Pharm 2: 1–11, 2012.
25. **YU D-F**, **JIANG S-J**, **PAN Z-P**, **CHENG W-D**, **ZHANG W-J**, **YAO X-K**, **LI Y-C**, **LUN Y-Z**. Expression and clinical significance of Sirt1 in colorectal cancer. Oncol Lett 11: 1167–1172, 2016. doi: 10.3892/ol.2015.3982.
26. **Tekin S**, **Beytur A**, **Cakir M**, **Taslıdere A**, **Erden Y**, **Tekin C**, **Sandal S**. Protective effect of saxagliptin against renal ischaemia reperfusion injury in rats. Arch Physiol Biochem 128: 608–618, 2022. doi: 10.1080/13813455.2020.1715442.
27. **Awadalla A**, **Hussein AM**, **El-Far YM**, **Barakat N**, **Hamam ET**, **El-Sherbiny**

M, **El-Shafey M**, **Shokeir AA**. Effect of zinc oxide nanoparticles and ferulic acid on renal ischemia/reperfusion injury: possible underlying mechanisms. Biomedicine & Pharmacotherapy 140: 111686, 2021. doi: 10.1016/j.biopha.2021.111686.

28. **Moin H**, **Shafi R**, **Ishtiaq A**, **Liaquat A**, **Majeed S**, **Zaidi NN**. Effectiveness of analog of Humanin in ameliorating streptozotocin-induced diabetic nephropathy in Sprague Dawley rats. Peptides (NY) 165: 171014, 2023. doi: 10.1016/j.peptides.2023.171014.
29. **Caio-Silva W**, **da Silva Dias D**, **Junho CVC**, **Panico K**, **Neres-Santos RS**, **Pelegrino MT**, **Pieretti JC**, **Seabra AB**, **De Angelis K**, **Carneiro-Ramos MS**. Characterization of the Oxidative Stress in Renal Ischemia/Reperfusion-Induced Cardiorenal Syndrome Type 3. Biomed Res Int 2020: 1–11, 2020. doi: 10.1155/2020/1605358.
30. **Martin JL**, **Gruszczyk A V.**, **Beach TE**, **Murphy MP**, **Saeb-Parsy K**. Mitochondrial mechanisms and therapeutics in ischaemia reperfusion injury. Pediatric Nephrology 34: 1167–1174, 2019. doi: 10.1007/s00467-018-3984-5.
31. **Kalpage HA**, **Bazylianska V**, **Recanati MA**, **Fite A**, **Liu J**, **Wan J**, **Mantena N**, **Malek MH**, **Podgorski I**, **Heath EI**, **Vaishnav A**, **Edwards BF**, **Grossman LI**, **Sanderson TH**, **Lee I**, **Huttemann M**. Tissue-specific regulation of cytochrome c by post-translational modifications: respiration, the mitochondrial membrane potential, ROS, and apoptosis. The FASEB Journal 33: 1540–1553, 2019. doi: 10.1096/fj.201801417R.
32. **Salahuddin Z**, **Rafi A**, **Muhammad H**, **Aftab U**, **Akhtar T**, **Zafar MS**, **Shahzad M**. Revolutionalizing the age old conventional treatment of psoriasis: An animal based comparative study between methylprednisolone and different doses of a novel anti-oxidant humanin analogue (HNG). Int Immunopharmacol 110: 108990, 2022. doi: 10.1016/j.intimp.2022.108990.
33. **Kumfu S**, **Charununtakorn ST**, **Jaiwongkam T**, **Chattipakorn N**, **Chattipakorn SC**. Humanin prevents brain mitochondrial dysfunction in a cardiac ischaemia–reperfusion injury model. Exp Physiol 101: 697–707, 2016. doi: 10.1113/EP085749.
34. **Yang H**, **Cui Y**, **Tang Y**, **Tang X**, **Yu X**, **Zhou J**, **Yin Q**, **Shentu X**. Cytoprotective role of humanin in lens epithelial cell oxidative stress-induced injury. Mol Med Rep 22: 1467–1479, 2020. doi: 10.3892/mmr.2020.11202.
35. **Zhang J**, **Lei H**, **Li X**. The protective effects of S14G-humanin (HNG) against mono-sodium urate (MSU) crystals- induced gouty arthritis. Bioengineered 13: 345–356, 2022. doi: 10.1080/21655979.2021.2001911.
36. **Gurunathan S**, **Jeyaraj M**, **Kang M-H**, **Kim J-H**. Mitochondrial Peptide Humanin Protects Silver Nanoparticles-Induced

Neurotoxicity in Human Neuroblastoma Cancer Cells (SH-SY5Y). Int J Mol Sci 20: 4439, 2019. doi: 10.3390/ijms20184439.

37. **Qin Q**, **Jin J**, **He F**, **Zheng Y**, **Li T**, **Zhang Y**, **He J**. Humanin promotes mitochondrial biogenesis in pancreatic MIN6 β-cells. Biochem Biophys Res Commun 497: 292–297, 2018. doi: 10.1016/j.bbrc.2018.02.071.
38. **Li L**, **Zhi D**, **Cheng R**, **Li J**, **Luo C**, **Li H**. The neuroprotective role of SIRT1/PGC-1α signaling in limb postconditioning in cerebral ischemia/reperfusion injury. Neurosci Lett 749: 135736, 2021. doi: 10.1016/j.neulet.2021.135736.
39. **Yu L**, **Gong B**, **Duan W**, **Fan C**, **Zhang J**, **Li Z**, **Xue X**, **Xu Y**, **Meng D**, **Li B**, **Zhang M**, **Bin Zhang**, **Jin Z**, **Yu S**, **Yang Y**, **Wang H**. Melatonin ameliorates myocardial ischemia/reperfusion injury in type 1 diabetic rats by preserving mitochondrial function: role of AMPK-PGC-1α-SIRT3 signaling. Sci Rep 7: 41337, 2017. doi: 10.1038/srep41337.
40. **Li Y**, **Jiao Y**, **Liu Y**, **Fu J**, **Sun L**, **Su J**. PGC-1α protects from myocardial ischaemia-reperfusion injury by regulating mitonuclear communication. J Cell Mol Med 26: 593–600, 2022. doi: 10.1111/jcmm.16236.
41. **Chen L**, **Qin Y**, **Liu B**, **Gao M**, **Li A**, **Li X**, **Gong G**. PGC-1α-Mediated Mitochondrial Quality Control: Molecular Mechanisms and Implications for Heart Failure. Front Cell Dev Biol 10, 2022. doi: 10.3389/fcell.2022.871357.
42. **Kim S-J**, **Guerrero N**, **Wassef G**, **Xiao J**, **Mehta HH**, **Cohen P**, **Yen K**. The mitochondrial-derived peptide humanin activates the ERK1/2, AKT, and STAT3 signaling pathways and has age-dependent signaling differences in the hippocampus. Oncotarget 7: 46899–46912, 2016. doi: 10.18632/oncotarget.10380.
43. **Gao G-S**, **Li Y**, **Zhai H**, **Bi J-W**, **Zhang F-S**, **Zhang X-Y**, **Fan S-H**. Humanin analogue, S14G-humanin, has neuroprotective effects against oxygen glucose deprivation/reoxygenation by reactivating Jak2/Stat3 signaling through the PI3K/AKT pathway. Exp Ther Med 14: 3926–3934, 2017. doi: 10.3892/etm.2017.4934.
44. **Yan B**, **Min S-J**, **Xu B**, **Zhang C**, **Pei J**, **Zhang W**, **Luo G-H**. The protective effects of exogenous spermine on renal ischemia-reperfusion injury in rats. Transl Androl Urol 10: 2051–2066, 2021. doi: 10.21037/tau-21-280.
45. **Kim KH**. Intranasal delivery of mitochondrial protein humanin rescues cell death and promotes mitochondrial function in Parkinson's disease. Theranostics 13: 3330–3345, 2023. doi: 10.7150/thno.84165.
46. **Li X**, **Chen W**, **Feng J**, **Zhao B**. The effects of HIF-1α overexpression on renal injury, immune disorders and mitochondrial apoptotic pathways in renal

ischemia/reperfusion rats. Transl Androl Urol 9: 2157–2165, 2020. doi: 10.21037/tau-20-918.

47. **Zhang Z**, **Yao L**, **Yang J**, **Wang Z**, **Du G**. PI3K/Akt and HIF-1 signaling pathway in hypoxia-ischemia (Review). Mol Med Rep 18 (4): 3547–3554, 2018. doi: 10.3892/mmr.2018.9375.
48. **Jiang N**, **Zhao H**, **Han Y**, **Li L**, **Xiong S**, **Zeng L**, **Xiao Y**, **Wei L**, **Xiong X**, **Gao P**, **Yang M**, **Liu Y**, **Sun L**. HIF-1α ameliorates tubular injury in diabetic nephropathy via HO-1–mediated control of mitochondrial dynamics. Cell Prolif 53, 2020. doi: 10.1111/cpr.12909.
49. **Cai H**, **Liu Y**, **Men H**, **Zheng Y**. Protective Mechanism of Humanin Against Oxidative Stress in Aging-Related Cardiovascular Diseases. Front Endocrinol (Lausanne) 12, 2021. doi: 10.3389/fendo.2021.683151.
50. **Means RE**, **Katz SG**. Balancing life and death: BCL-2 family members at diverse ER–mitochondrial contact sites. FEBS J 289: 7075–7112, 2022. doi: 10.1111/febs.16241.
51. **Lue Y**, **Gao C**, **Swerdloff R**, **Hoang J**, **Avetisyan R**, **Jia Y**, **Rao M**, **Ren S**, **Atienza V**, **Yu J**, **Zhang Y**, **Chen M**, **Song Y**, **Wang Y**, **Wang C**. Humanin analog enhances the protective effect of dexrazoxane against doxorubicin-induced cardiotoxicity. American Journal of Physiology-Heart and Circulatory Physiology 315: H634–H643, 2018. doi: 10.1152/ajpheart.00155.2018.
52. **Morris DL**, **Johnson S**, **Bleck CKE**, **Lee D-Y**, **Tjandra N**. Humanin selectively prevents the activation of pro-apoptotic protein BID by sequestering it into fibers. Journal of Biological Chemistry 295: 18226–18238, 2020. doi: 10.1074/jbc.RA120.013023.